Design of Advanced Thermoelectric Materials

Shaabani, Laaya

Chapter 6

High temperature ferromagnetism in Ce-doped PbSe

Abstract

We present a systematic study of the magnetic properties of PbSe doped with Ce. Lead selenide doped with Ce ($Pb_{1-x}Ce_xSe$, x = 0.00, 0.01, 0.02, 0.03 and 0.05) have been synthesized by the solid state reaction method. We have observed a high temperature ferromagnetic signal in lightly doped samples ($x \leq 0.03$ Ce-doped). The saturation magnetization of the samples decreases with increasing dopant concentration. A Curie temperature of 780 K is obtained for $Pb_{0.99}Ce_{0.01}Se$. The ferromagnetism probably arises from CeO_2 nanoparticles embedded in the PbSe matrix.

6.1 Introduction

Dilute magnetic semiconductors (DMS) have drawn a great deal of attention in recent years due to their possible applications in spintronic devices and optoelectronics.[1-4] DMS compounds are typically magnetic semiconducting materials, such as II–VI, IV–VI, II-V or III-V compounds, in which some metal ions have been replaced by magnetic rare-earth (RE) or transition metal (TM) ions.[5] A large number of studies has been reported on II–VI compounds such as CdTe, ZnTe, HgTe materials containing Mn, Co and Fe ions and the corresponding selenides and sulfides over the last two decades.[6,7] A smaller number of studies have also reported magnetization, magnetic susceptibility and electron paramagnetic resonance (EPR) measurements of IV–VI semiconductors doped with rare earth or transition metal impurities.[8-15] For instance, it has been reported that room-temperature ferromagnetism (RTFM) is observed in Ni, Cr and Ge/Cr doped PbTe.[13-15] However, little attention has so far been paid to the magnetic properties of PbSe doped with rare earth elements.[12,16-18] There is increasing interest in the search for ferromagnetic semiconductors with a Curie temperature (T_C) above room temperature, which could be used for advanced spin electronics applications. In this work, we present results on the influence of Ce doping on the magnetic properties of PbSe. We report ferromagnetism in lightly doped $Pb_{1-x}Ce_xSe$ ($x \leq 0.03$) alloys with a Curie temperature as high as 780 K and discuss possible origins of this behavior.

6.2 Experimental section

6.2.1 Sample fabrication

Synthesis. The $Pb_{1-x}Ce_xSe$ alloys with x = 0.00, 0.01, 0.02, 0.03 and 0.05 were synthesized by the solid state reaction method. The elements used as starting materials were Pb (99.999%, Aldrich), Se (99.5%, Alfa Aesar) and Ce (99.99%, Alfa Aesar).

Stoichiometric amounts of the elements were weighed and, after grinding for 20 min, transferred to a clean quartz ampoule and sealed under vacuum. The sealed ampoule was slowly heated to 723 K over 12 h, heated further to 1273 K over 7 h, held at this temperature for 6 h and followed by an air quench. The ingots of the samples were taken out of the ampoules and were then ground thoroughly for 1 h to obtain a fine powder. Afterwards, the powder from each sample was loaded into a 5 mm die and pressed under 5 t/cm^2 to obtain cylindrical pellets.

6.2.2 Transport properties measurements

Seebeck coefficient and resistivity measurements. Electrical conductivity (σ) and Seebeck coefficient (S) were simultaneously measured using a Linseis LSR-3 instrument. Measurements were performed under helium atmosphere from room temperature to 823 K. The disk-shaped samples were cut and polished into parallelepiped shapes for these measurements.

Characterizations. X-ray diffraction (XRD) measurements were performed using a Bruker D8 Advance diffractometer with Cu (Kα) radiation (λ = 1.5406 Å) at room temperature. The magnetic properties of the samples were characterized using a Quantum Design MPMS XL-7 superconducting quantum interface device (SQUID) magnetometer.

Electron microscopy analysis. The microstructures of the samples were studied using a high resolution scanning electron microscope (SEM), JEOL JSM-7001 and the TEM-EDX was performed using a JEOL 2010F transmission electron microscope (TEM) operated at 200 kV.

6.3 Results and discussion

6.3.1 PXRD patterns

The powder x-ray diffraction patterns of the $Pb_{1-x}Ce_xSe$ (x = 0.01, 0.02, 0.03, and 0.05) ingots are shown in Figure 6.1. Diffraction patterns of the undoped PbSe ingots are also given for comparison. All the samples are crystalized in the face-centered-cubic (FCC) rocksalt (NaCl) structure, but additional weak peaks are observed in the XRD patterns of the samples at cerium concentrations above x = 0.01. The impurity phase is identified as CeO_2. In order to obtain the lattice parameters, X-ray diffraction patterns were refined by Rietveld method within the $Fm\bar{3}m$ space group. The lattice parameter of all samples are 6.1268-6.1296 Å with an error of 0.0001 (Table. 6.1). There is no clear variation of lattice parameter with dopant concentration, which suggests that very little cerium is genuinely incorporated in the rocksalt lattice.

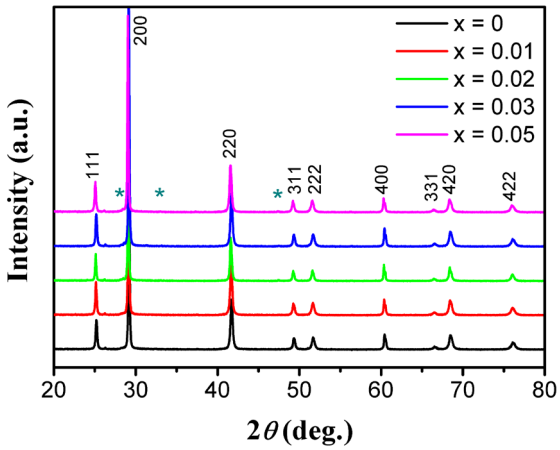

Figure 6.1: Powder X-ray diffraction patterns of $Pb_{1-x}Ce_xSe$ samples with different Ce concentrations of x = 0, 0.01, 0.02, 0.03, and 0.05 at 300 K. Stars indicate peaks from the secondary phase.

Table 6.1: Lattice parameters of $Pb_{1-x}Ce_xSe$ (x = 0, 0.01, 0.02, 0.03, and 0.05) compounds

Sample name	Lattice parameter(Å)
	a
PbSe	6.1281(1)
$Pb_{0.99}Ce_{0.01}Se$	6.1271(1)
$Pb_{0.98}Ce_{0.02}Se$	6.1313(1)
$Pb_{0.97}Ce_{0.03}Se$	6.1296(1)
$Pb_{0.95}Ce_{0.05}Se$	6.1268(1)

6.3.2 Magnetic properties

Figures 6.2a-6.2c show the magnetic susceptibility of the samples as a function of temperature, where M is the measured magnetization and H is the magnetic field. A curve typical of ferromagnetic order is observed for samples with low cerium content (x = 0.01 and 0.03), whereas the undoped sample is diamagnetic. A correction for the diamagnetic susceptibility of the PbSe matrix was applied to all presented data.[19] The temperature dependence of the susceptibility for the x = 0.03 doped sample is similar to that observed for the x = 0.01 sample, but the magnitude of the susceptibility is approximately 3 times smaller at 300K. The temperature dependence of the susceptibility measured at 5000Oe for the x = 0.05 doped sample shows typical paramagnetic behavior below room temperature (Figure 6.2c). The inset in Figure 6.2c illustrates that the temperature dependence of the inverse susceptibility for x = 0.05, ($1/\chi$) can be fitted using the Curie-Weiss law. This indicates that Ce ions form a system of non-interacting localized magnetic moments. The resulting effective magnetic moment per Ce atom is 0.23 μ_B, which is lower than the value of 2.54 μ_B expected for Ce^{3+}.[20]

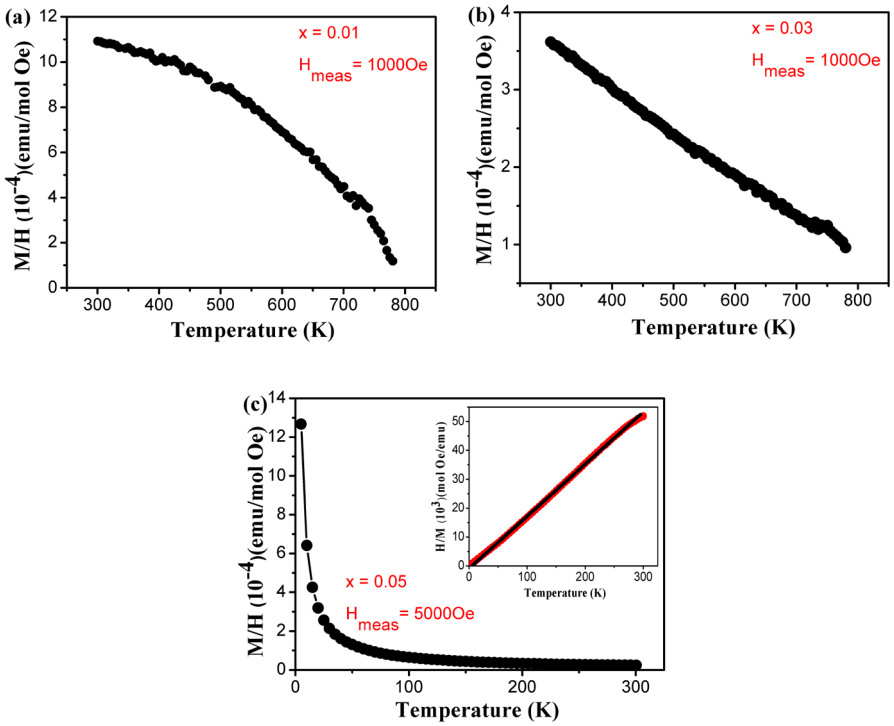

Figure 6.2: (a) Temperature dependence of magnetic susceptibility measured in an applied field of 1000 Oe for (a) $Pb_{0.99}Ce_{0.01}Se$ and (b) $Pb_{0.97}Ce_{0.03}Se$. (c) Temperature dependence of magnetic susceptibility measured in an applied field of 5000 Oe for $Pb_{0.95}Ce_{0.05}Se$. The inset shows a fit to the inverse susceptibility using the Curie-Weiss law.

To further investigate the magnetic properties of these samples, the magnetization (M) of all samples was measured versus applied magnetic field (H) at 300 K (Figure 6.3). The magnetization hysteresis loops for the $x = 0.01$ and $x = 0.03$ samples clearly demonstrate ferromagnetic behavior, which is in agreement with the previously presented magnetic susceptibility results. On the contrary, a linear dependence of the magnetization is observed for the $x = 0.05$ doped sample. The largest magnetization is obtained for the $Pb_{0.99}Ce_{0.01}Se$ sample (5.2×10^{-3} emu g^{-1}), and the magnetization of the samples decreases with increasing Ce content until a paramagnetic response is observed for $x = 0.05$.

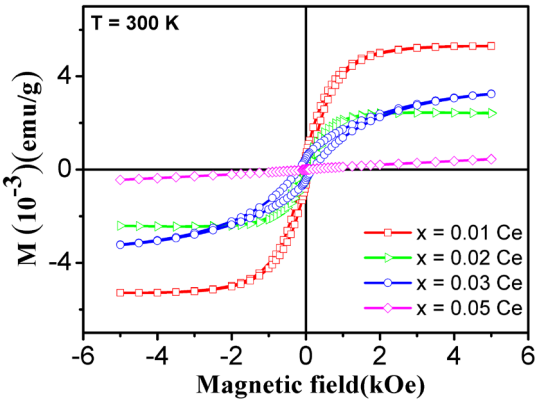

Figure 6.3: Magnetization as function of applied magnetic field for $Pb_{1-x}Ce_xSe$ samples (x = 0, 0.01, 0.02, 0.03, and 0.05) measured at 300 K.

Figures 6.4a and 6.4b show more detailed views of the magnetization versus applied magnetic field for x = 0.01 and x = 0.03, where hysteresis loops are visible at temperatures between 25 K and 650 K. The saturation magnetization increases as the temperature is reduced. The ferromagnetic Curie temperature, T_C, is estimated as 780 K by extrapolating the steep high temperature part of the susceptibility versus temperature plot.

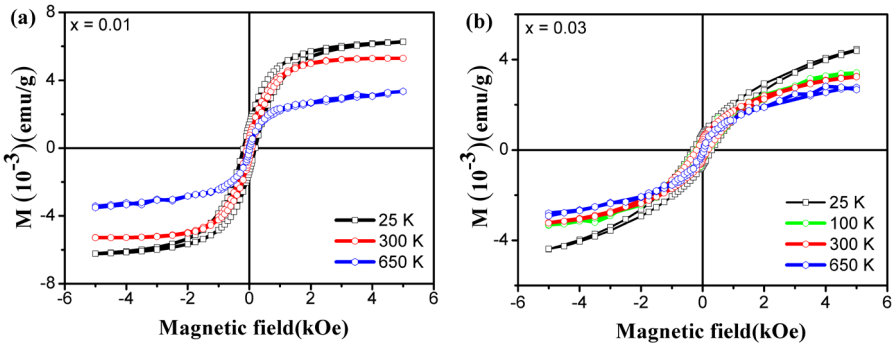

Figure 6.4: (a) Magnetization as a function of applied magnetic field for $Pb_{0.99}Ce_{0.01}Se$ measured at various constant temperatures of 25 K, 300 K and 650 K in a magnetic field of up to 5 kOe. (b) Magnetization versus applied field for $Pb_{0.97}Ce_{0.03}Se$ at various constant temperatures of 25 K, 100 K, 300 K and 650 K in an applied magnetic field of up to 5 kOe.

6.3.3 Microstructural properties

To investigate the origin of the ferromagnetism, transmission electron microscopy was performed on the $Pb_{0.99}Ce_{0.01}Se$ sample, which showed the strongest magnetic response. A piece of the ingot was ground finely and dispersed on a carbon grid coated with a holey carbon film. The TEM images revealed agglomerates of particles with typical sizes much smaller than 100 nm. Energy dispersive X-ray analysis (EDX) was performed on a number of different particles and agglomerates in an effort to probe the chemical homogeneity of the sample and the distribution of the Ce dopant. Some examples of EDX analysis on different particles are shown in Figure 6.5 and 6.6, where Ce-rich regions were found. For example, in Figure 6.5a there is an overall Pb:Se ratio of 1:1 in the ~2 × 2 μm agglomerate as expected for PbSe, but Ce accounts for ~10 mole%, far more than the nominal doping level of 1%. Area 1 in Figure 6.5a appears to be pure PbSe, whereas areas 2 and 3 (diameter ~400 nm) differ little in composition from the overall agglomerate of particles. No obvious inclusions can be distinguished in these areas, suggesting that Ce is either incorporated evenly in the PbSe matrix or that any Ce-rich regions are extremely small. In all regions of Figure 6.5a that contain Ce, including areas 2 and 3, there is also a significant concentration of oxygen. Although the quantitative analysis of oxygen by EDX is less accurate than the heavier elements, it is likely that most of the cerium exists in the form of an oxide phase. In other parts of the sample some larger Ce-rich particles were found; the largest that was observed is shown in Figure 6.5b which is ~2 μm across and from the EDX analysis appears to be pure cerium oxide. Similarly, Figure 6.6 shows a cerium oxide particle of ~200 nm in size adjacent to a PbSe particle. Varying lighter and darker contrast in regions smaller than 10 nm can be observed within the cerium oxide particle in Figure 6.6c, suggesting that it might consist of a cluster of nanoparticles.

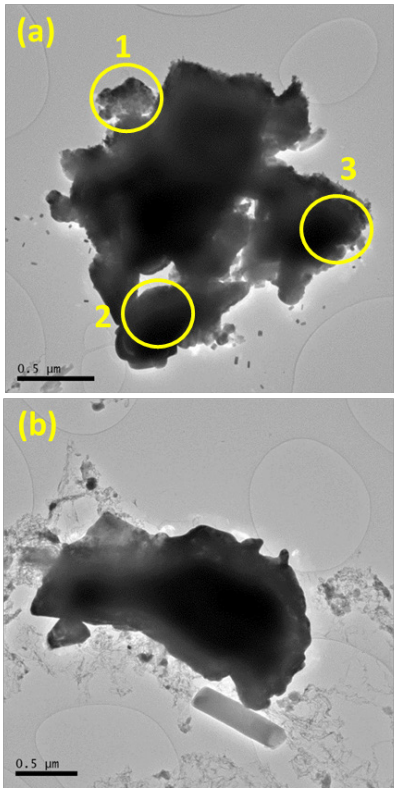

Area	Pb%	Se%	Ce%	O%
Image (a)	35.0(4)	35.0(5)	10.6(3)	19.4(9)
1	55.6(7)	42.1(7)	0	2.3(6)
2	42.2(4)	32.1(4)	11.7(3)	14.0(9)
3	38.9(4)	29.8(4)	14.7(2)	16.6(11)

Area	Pb%	Se%	Ce%	O%
Image (b)	0.40(8)	0.09(10)	57.0(6)	42.5(18)

Figure 6.5: TEM images and EDX analysis of $Pb_{0.99}Ce_{0.01}Se$. (a) Agglomerate of particles containing ~10 molar% Ce; EDX analysis was performed on the circled areas as well as the overall area of the image. (b) The largest Ce-rich particle that was observed in the sample, seemingly comprised of pure cerium oxide.

Based on the TEM analysis, it is probable that the ferromagnetic response in $Pb_{0.99}Ce_{0.01}Se$ and $Pb_{0.97}Ce_{0.03}Se$ arises from small cerium oxide particles. Ferromagnetism has previously been observed in CeO_2 nanoparticles smaller than 20 nm, with T_C in the vicinity of room temperature.[21] Here the saturation magnetization was an order of magnitude larger than in our samples, approaching 0.1 emu/g. In another study Ge et al. reported ferromagnetism in CeO_2 nanocubes of 5nm size, where the saturation magnetization of 0.006 emu/g was similar to our samples.[22] Here it was suggested that oxygen vacancies migrate to the surface of the nanoparticles, where uncompensated 4f spins surrounding the vacancies are

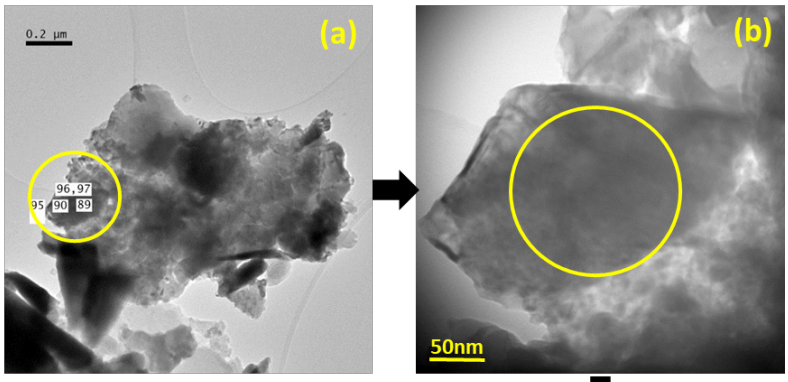

Area	Pb%	Se%	Ce%	O%
Image (b)	1.1(2)	0.7(2)	62.8(5)	35.3(12)

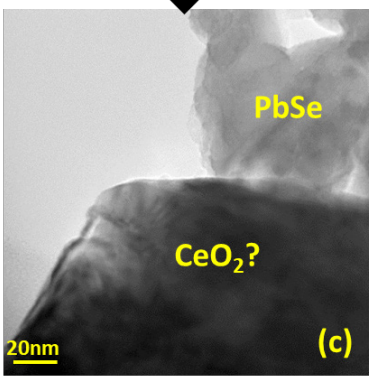

Figure 6.6: TEM images and EDX analysis of $Pb_{0.99}Ce_{0.01}Se$. (a) Agglomerate of particles, where the yellow circled area is Ce-rich and shown in more detail in (b). This region is zoomed in closer in (c), where an apparent boundary between cerium oxide and PbSe particles can be observed.

responsible for the ferromagnetic signal; particles of 100 nm showed a much weaker ferromagnetic signal. Ackland et al. later reported on ferromagnetism in CeO_2 nanoparticles of size 4 nm and calculated that only 0.15% of the sample volume is magnetic.[23] This was attributed to two possible mechanisms: either charge transfer magnetism involving the formation of an impurity band that can be spontaneously spin-split due to the Stoner criterion, or so-called giant orbital paramagnetism at the nanoparticle surface where a huge orbital moment is formed by coulomb correlation in a 2D electron gas in response to an applied magnetic field. The latter mechanism was subsequently deemed to be most likely in a follow-up study,[24] and it was shown

that this phenomenon can occur in nanoparticles below ~100 nm in size and can exist to well above room temperature.

One must also consider the possibility of the presence of trace amounts of other ferromagnetic impurities in the sample that might be below the sensitivity of EDX measurements. This aspect requires further careful investigation. However, the observation that the ferromagnetism disappears when Ce is doped at the nominal level of 5% using identical experimental procedures, and where larger Ce-rich particles are likely formed, suggests that the ferromagnetic signal arises not from the starting materials or from sample contamination but from very small cerium oxide inclusions when the nominal doping level is low.

A very recent study by Zhao et al. showed that the presence of magnetic nanoparticles in a thermoelectric matrix can have a beneficial effect on the thermoelectric properties.[25] Superparamagnetic nanoparticles of Co (up to 0.3 atom%) were embedded in the thermoelectric material $Ba_{0.3}In_{0.3}Co_4Sb_{12}$, and improved ZT by up to 40%. This result was attributed to three effects of the nanoparticles: charge transfer to the matrix, increasing the carrier concentration; scattering of the conduction electrons by the magnetic moments, which decreases the mobility and increases the Seebeck coefficient; enhancing the phonon scattering by the magnetic moments. This strongly suggests that the presence of magnetic impurities such as the CeO_2 in our doped PbSe samples is not necessarily a bad thing, and that such "impure" samples with weak magnetic moments are worth investigating in more detail for possible enhanced thermoelectric performance.

6.3.4 Electrical resistivity, Seebeck coefficient and power factor

The temperature dependent Seebeck coefficient and electrical resistivity of the $Pb_{1-x}Ce_xSe$ (x = 0.01, 0.03 and 0.05) samples in the temperature range of 300-820 K were measured and the results are compared with the undoped sample in Figure 6.7a-6.7c. The electrical resistivity generally increases with increasing Ce content, although the electrical resistivity of the sample with x = 0.03 is much higher than the other samples below 500 K. As a result, the power factor decreases for the doped samples (Figure 6.7c). These results indicate that adding Ce at levels above 1% to the PbSe matrix has no beneficial effect on enhancing the electrical properties (Seebeck coefficient and electrical conductivity), probably because the solubility limit of Ce is quickly reached and excess Ce is incorporated into the precipitate phase instead of entering the PbSe lattice. For further inspection, microstructural analysis of the samples was conducted by scanning electron microscopy (SEM) as shown in Figures 6.8-6.10. In the matrix of PbSe, CeO_2 precipitates were found as large of tens of µm, indicating that excess Ce doping induces the formation of secondary phase impurities. The precipitates appear to vary with respect to the Ce concentration, an interesting point is that in the x = 0.05 sample there is less CeO_2 compared with the two other samples (Figure 6.10). Although the largest magnetization is obtained for the x = 0.01 sample, the concentration of CeO_2 in this sample is lower than in the x = 0.03 sample. Having the highest concentration of precipitates in the sample with x = 0.03 (Figure 6.9) is consistent with the highest electrical resistivity for this sample. Furthermore, there is a large concentration of lead silicon oxide impurities at the grain boundaries of this sample, which suggests that PbO reacted with the walls of the quartz tube (SiO_2) and produced a compound which has a lower melting point and stays at the grain boundaries. This suggests that the deterioration in both the Seebeck coefficient and electrical resistivity with doping results from these impurities.

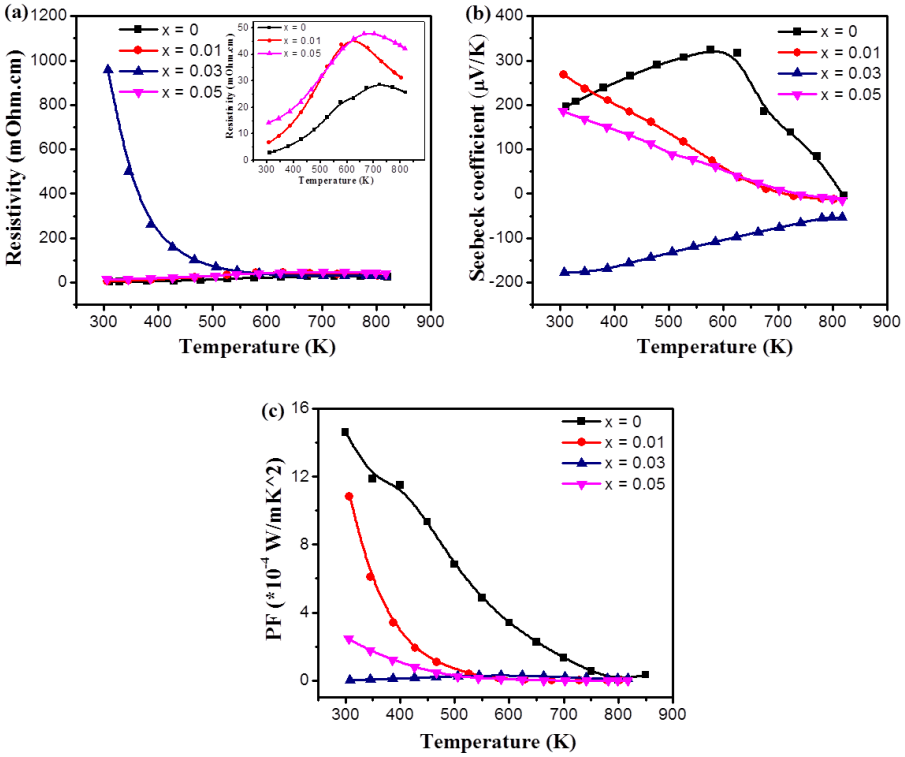

Figure 6.7: Temperature dependence of (a) electrical resistivity, (b) Seebeck coefficient, and (c) power factor for $Pb_{1-x}Ce_xSe$ samples (x = 0, 0.01, 0.03, and 0.05). The inset shows a closer view of electrical resistivity as a function of temperature for samples with x = 0, 0.01, and 0.05.

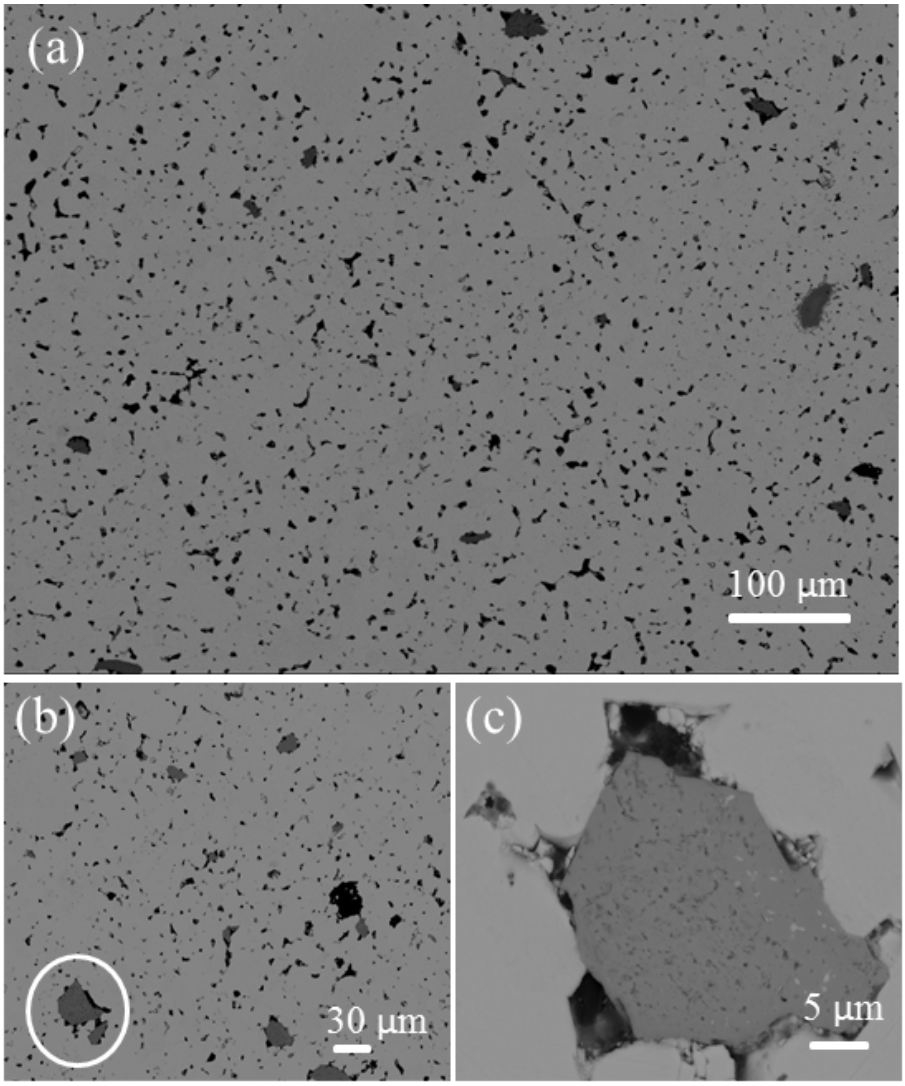

Figure 6.8: (a) SEM image of $Pb_{0.99}Ce_{0.01}Se$ sample, showing the morphology and the distribution of precipitates in the matrix. (b) CeO_2 precipitates distributed within the PbSe matrix. (c) Closer view of the same CeO_2 precipitate in the PbSe matrix.

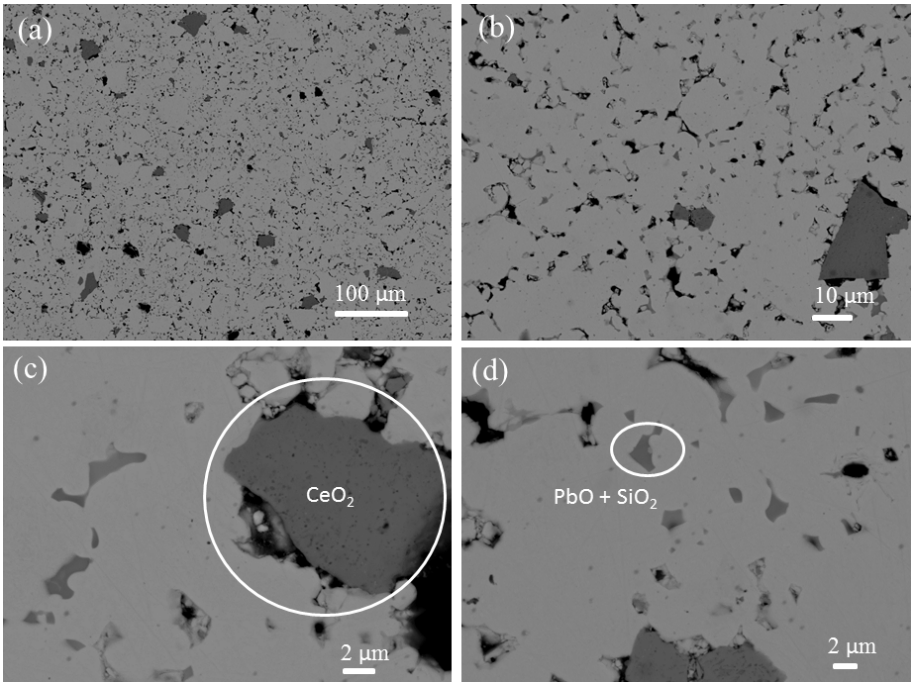

Figure 6.9: (a)-(b) SEM images of $Pb_{0.97}Ce_{0.03}Se$ sample, showing the morphology and the distribution of precipitates in the matrix. (c) CeO_2 precipitates distributed within the PbSe matrix. (d) $PbO+SiO_2$ marked by the white circle.

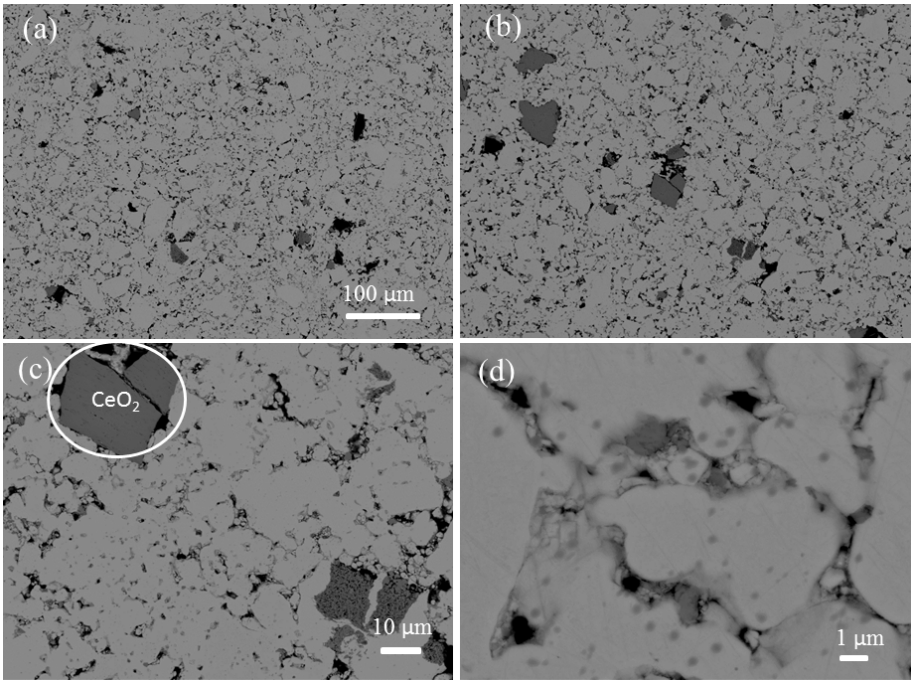

Figure 6.10: (a)-(b) SEM images of $Pb_{0.95}Ce_{0.05}Se$ sample, showing the morphology and the distribution of precipitates in the matrix. (c) CeO_2 precipitates distributed within the PbSe matrix. (d) Closer view of CeO_2 precipitates in the PbSe matrix.

6.4 Conclusion

We have performed a detailed study on the effect of Ce doping on the magnetic properties of PbSe. It was found that lightly doped $Pb_{1-x}Ce_xSe$ ($x \leq 0.03$) alloys exhibit high temperature ferromagnetism. The ferromagnetic response of the x = 0.01 doped sample was found to be highest at room temperature with a saturation magnetization of about 5.2 memu/g, and the magnetization of the samples decreases with Ce content. TEM and SEM images suggested that cerium is mainly found in the form of cerium oxide inclusions, which if small enough can be responsible for the ferromagnetic signal. For future studies it is possible that controlling the

size and distribution of the ferromagnetic impurity inclusions might enhance the thermoelectric performance, but at Ce doping levels less than 1%.

Bibliography

1. G. A. Prinz, Magnetoelectronics. *Science* **1998**, 282, 1660.

2. P. Ball, Meet the spin doctors. *Nature* **2000**, 404, 918.

3. S. A. Wolf, D. D. Awschalom, R. A. Buhrman, J. M. Daughton, S. von Moln´ar, M. L. Roukes, A. Y. Chtchelkanova, and D. M. Treger, Spintronics: A spin-based electronics vision for the future. *Science* **2001**, 294, 1488.

4. J. Liu, L. Chen, H. N. Dong, and R. L. Zheng, First-principle study on the magnetic properties of six potential half-metallic ferromagnets: C-doped alkaline-earth chalcogenides. *Appl. Phys. Lett.* **2009**, 95, 132502.

5. K. Sato, L. Bergqvist, J. Kudrnovský, P. H. Dederichs, O. Eriksson, I. Turek, B. Sanyal, G. Bouzerar, H. Katayama-Yoshida, V. A. Dinh, T. Fukushima, H. Kizaki, and R. Zeller, First-principles theory of dilute magnetic semiconductors. *Reviews of modern Phys.* **2010**, 82, 1633.

6. J. K. Furdyna, Diluted magnetic semiconductors. *J. Appl. Phys.* 1988, 64, 29.

7. J. K. Furdyna, Diluted magnetic semiconductors: Issues and opportunities. *J. Vac. Sci. Technol. A4* **1986**, 2002.

8. F. T. Hedgcock, P. C. Sullivana, J. T. Grembowicz, and M. Bartkowski, Magnetic properties of Gd-doped PbTe. *Can. J. Phys.* **1986**, 64,1345.

9. J. Heremans and D. L. Partin. Magnetic properties of EuTe-PbTe superlattices. *Phys. Rev. B* **1988**, 37,6311.

10. M. Gorska and J. R. Anderson, Magnetic susceptibility and exchange in IV-VI compound diluted magnetic semiconductors. *Phys. Rev. B* **1988**, 38, 13, 9120.

11. D. M. Zayachuk, V. I. Mikityuk, A. V. Pashuk, V. V. Shlemkevych, K. S. Ulyanitsky, and D. Kaczorowski, Specific magnetic properties of the Eu-doped PbTe single crystals. *J. Physical studies* **2012**, 16, 1/2,1703.

12. V. Jovovic, S. J. Thiagarajan, J. West, J. Heremans, T. Story, Z. Golacki, W. Paszkowicz, and V. Osinniy, Transport and magnetic properties of dilute rare-earth–PbSe alloys. *J. Appl. Phys.* **2007**, 102, 043707.

13. N. Romcevic, J. Trajic, M. Romcevic, D. Stojanovic, T. A. Kuznetsova, D. R. Khokhlov, W. Dobrowolski, R. Rudolfd, and I. Anzel, Optical and Magnetic Properties of PbTe(Ni). *Acta Phys. Polonica A* **2009**, 115, 805.

14. E. A. Zvereva, E. P. Skipetrov, O. A. Savelieva, N. A. Pichugin, A. E. Primenko, E. I. Slyn'ko, and V. E. Slyn'ko, Room-temperature ferromagnetism in diluted magnetic semiconductor $Pb_{1-x}Cr_xTe$. *Journal of Physics: Conference Series* **2010**, 200, 062039.

15. E. P. Skipetrov, M. G. Mikheev, F. A. Pakpour, L. A. Skipetrova, N. A. Pichugin, E. I. Slyn'ko, and V. E. Slyn'ko, Ferromagnetism in diluted $Pb_{1-x-y}Ge_xCr_yTe$ magnetic semiconductors. *Semiconductors* **2009**, 43, 3, 297.

16. S. Isber, S. Charar, C. Fau, V. Mathet, and M. Averous, EPR spectra and magnetization of Eu^{2+} ions in PbSe. *Phys. Rev. B* **1995**, 52, 3, 1678.

17. X. Gratens, S. Isber, S. Charar, and Z. Golacki, Magnetic susceptibility study of Ce^{3+} in PbCeA (A=Te, Se, S). *J. Magnetism and Magnetic Materials* **2012**,324, 2761.

18. X. Song, S. Dong, and H. Zhao, First principles study of structural, magnetic and electronic properties of PbX (X= S and Se) doped with B, C and N. *Journal of Superconductivity and Novel Magnetism* **2013**, 26, 3437.

19. G. A. Bain and J. F. Berry, Diamagnetic corrections and Pascal's constants. *Journal of Chemical Education* **2008**, 85, 4, 532.

20. E. M. Levin, B. A. Cook, J. L. Harringa, S. L. Bud'ko, R. Venkatasubramanian, and K. Schmidt-Rohr, Analysis of Ce- and Yb-Doped TAGS-85 materials with enhanced thermoelectric figure of Merit. *J. Adv. Funct. Mater.* **2011**, 21, 441.

21. Y. Liu, Z. Lockman, A. Aziz, and J. MacManus-Driscoll, Size dependent ferromagnetism in cerium oxide (CeO_2) nanostructures independent of oxygen vacancies. *J. Phys. Condens. Matter.* **2008**, 20, 165201.

22. M. Y. Ge, H. Wang, E. Z. Liu, J. F. Liu, J. Z. Jiang, Y. K. Li, Z. A. Xu, and H. Y. Li, On the origin of ferromagnetism in CeO_2 nanocubes. *Appl. Phys. Lett.* **2008**, 93, 062505.

23. K. Ackland, L. M. A. Monzon, M. Venkatesan, and J. M. D. Coey, Magnetism of nanostructured CeO_2. *IEEE Trans. Magnetics* **2011**, 47, 3509.

24. M. Coey, K. Ackland, M. Venkatesan, and S. Sen, Collective magnetic response of CeO_2 nanoparticles. *Nature Phys.* **2016**, 12, 694.

25. W. Zhao, Z. Liu, Z. Sun, Q. Zhang, P. Wei, X. Mu, H. Zhou, C. Li, S. Ma, D. He, P. Ji, W. Zhu, X. Nie, X. Su, X. Tang, B. Shen, X. Dong, J. Yang, Y. Liu, and J. Shi, Superparamagnetic enhancement of thermoelectric performance. *Nature*, **2017**, 549, 247.